



CHORUS

This is the accepted manuscript made available via CHORUS. The article has been published as:

Ballistic Graphene Josephson Junctions from the Short to the Long Junction Regimes

I. V. Borzenets, F. Amet, C. T. Ke, A. W. Draelos, M. T. Wei, A. Seredinski, K. Watanabe, T. Taniguchi, Y. Bomze, M. Yamamoto, S. Tarucha, and G. Finkelstein

Phys. Rev. Lett. **117**, 237002 — Published 2 December 2016

DOI: [10.1103/PhysRevLett.117.237002](https://doi.org/10.1103/PhysRevLett.117.237002)

Ballistic graphene Josephson junctions from the short to the long junction regime

I. V. Borzenets^{1*}, F. Amet², C. T. Ke³, A. W. Draelos³, M. T. Wei³, A. Seredinski³, K. Watanabe⁴, T. Taniguchi⁴, Y. Bomze³, M. Yamamoto^{1,5}, S. Tarucha^{1,6}, G. Finkelstein³

¹*Department of Applied Physics, University of Tokyo, Bunkyo-ku, Tokyo 113-8656, Japan.*

²*Department of Physics and Astronomy, Appalachian State University, Boone, NC 28607, USA.*

³*Department of Physics, Duke University, Durham, NC 27708, USA.*

⁴*Advanced Materials Laboratory, National Institute for Materials Science, Tsukuba, 305-0044, Japan.*

⁵*PRESTO, JST, Kawaguchi-shi, Saitama 332-0012, Japan.*

⁶*Center for Emergent Matter Science (CEMS), RIKEN, Wako-shi, Saitama 351-0198, Japan.*

*Correspondence should be sent to I.V.B. (email: ivan@meso.t.u-tokyo.ac.jp)

We investigate the critical current, I_C , of ballistic Josephson junctions made of encapsulated graphene/boron-nitride heterostructures. We observe a crossover from the short to the long junction regimes as the length of the device increases. In long ballistic junctions, I_C is found to scale as $\propto \exp(-k_B T / \delta E)$. The extracted energies δE are independent of the carrier density and proportional to the level spacing of the ballistic cavity, as determined from Fabry-Perot oscillations of the junction normal resistance. As $T \rightarrow 0$ the critical current of a long (or short) junction saturates at a level determined by the product of δE (or Δ) and the number of the junction's transversal modes.

PACS numbers: 74.45.+c, 72.80.Vp, 74.50.+r, 73.23.-b

Encapsulated graphene/boron-nitride heterostructures emerged in the past year as a medium of choice for studying proximity-induced superconductivity in the ultra-clean limit [1–4]. These junctions support the ballistic propagation of superconducting currents across micron-scale graphene channels, and their critical current is gate-tunable across several orders of magnitude. In these devices, a rich phenomenology arises from the interplay of superconductivity with ballistic transport [1], cyclotron motion [2], and even the quantum Hall effect at high magnetic field [4].

In a superconductor - normal metal - superconductor (SNS) junction, single particles in the N region cannot enter the superconductor and therefore experience Andreev reflections at each S-N interface. This results in Andreev bound states (ABS), which are capable of carrying superconducting current across the N region. In long ballistic junctions, the energy spectrum of the ABS is quantized with a level spacing of $E_0 = \pi \hbar v_F / L$, where L is the junction length and v_F the Fermi velocity [5–9]. The energy of ABS cannot exceed the superconducting gap Δ , so in the short junction regime, $L \lesssim \xi \equiv \hbar v_F / \Delta$, only a single ABS remains.

In this work we study several ballistic junctions of different length and demonstrate that the temperature dependence of the critical current dramatically differs in the long and short regimes. For long junctions, we observe an exponential scaling of the current through the junction $I_C \propto \exp(-k_B T / \delta E)$, where $\delta E \approx \hbar v_F / 2\pi L$ [5, 6, 10, 11]. Note that in graphene v_F is a constant, and δE is expected to be independent of the carrier density or the mobility (as long as the junction remains ballistic.) For comparison, in a short junction we observe a different scaling, as expressed in eq. (1), in excellent agreement with the theory [12–14].

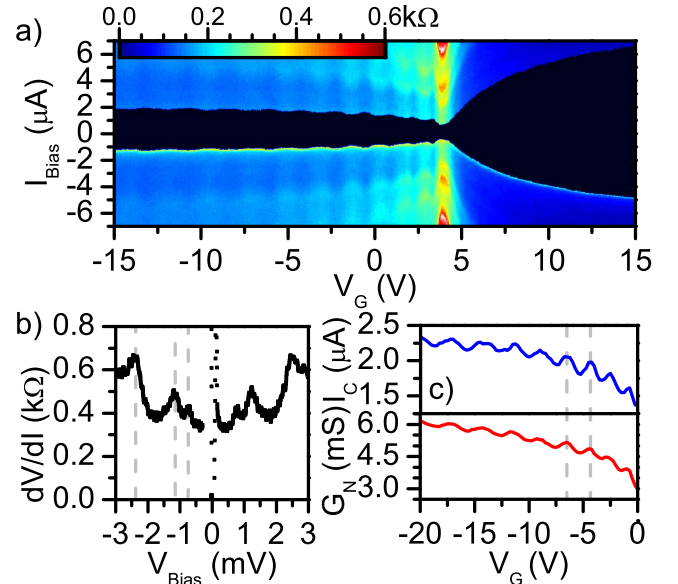


FIG. 1. a) Map of differential resistance versus current I and gate voltage V_G . The data are shown for Junction A and taken at a temperature $T = 1.5K$. The superconducting region of zero resistance can be observed around $I = 0$. The current through the junction is swept from negative to positive; therefore, the transition at the negative I corresponds to the retrapping current I_R , while the transition at the positive I corresponds to the switching current I_S . b) Differential resistance versus bias voltage (V_B) for Junction A taken at Dirac point. Several multiple Andreev reflection (MAR) peaks are observed: 2Δ , Δ , $2/3\Delta$; with $\Delta \approx 1.2\text{meV}$. c) The critical current I_C (top) and the normal conductance of the junction (bottom) plotted vs. gate voltage V_G in the hole conduction regime. Both quantities demonstrate Fabry-Perot oscillations and are roughly proportional to each other.

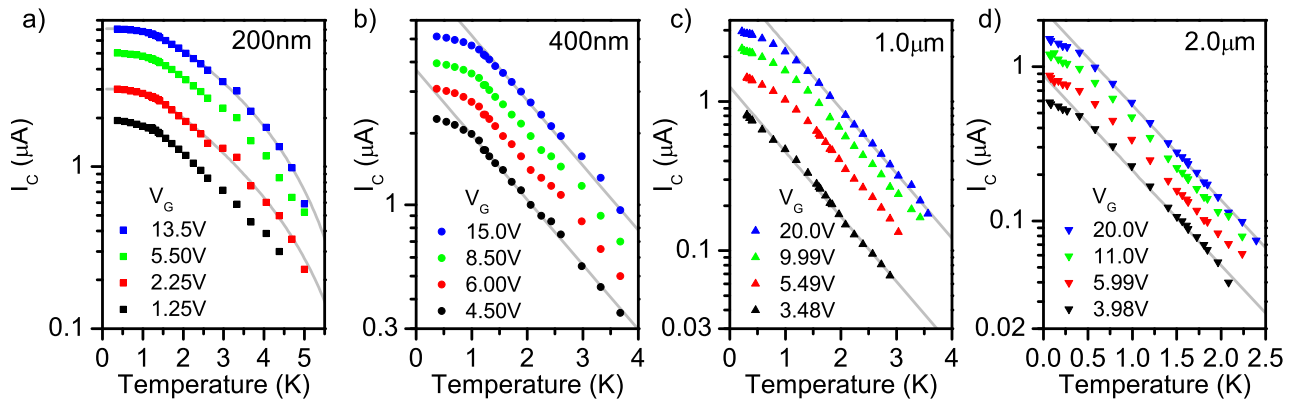


FIG. 2. Critical currents I_C plotted on a semi-log scale versus temperature T for Junctions A-D. Several gate voltages are presented for each junction; the values of V_G are shown relative to the Dirac point. a) The data for the shortest junction, A ($L = 200$ nm). The gray lines are fitted according to eq. (1), using the superconducting gap Δ extracted in Figure 1b. b-d) I_C vs. T for Junctions B-D respectively (see Supplementary for Junctions E, F, G). The slope of $\log(I_C)$ vs. T is independent of V_G . In the case of long ballistic graphene junctions, the inverse slope δE is expected to be independent of the carrier density and inversely proportional to L .

Our graphene layers are exfoliated from Kish graphite and encapsulated in hexagonal boron-nitride (hBN) using the “pick-up” method [15]. Heating beyond 250°C causes bubbles of trapped adsorbates to migrate towards the edges of the graphene mesa, effectively cleaning it. The edges of the graphene flake are exposed by etching through the hBN-graphene-hBN stack with a CHF_3/O_2 plasma (flow rates 40/6 sccm) at 1Pa and 60W power. The etching time varies depending on the thickness of the top hBN layer. We use DC magnetron sputtering to form Molybdenum-Rhenium alloy contacts (50/50 wt%), with a measured superconducting gap $\Delta_0 \approx 1.2\text{meV}$ (Figure 1b). These contacts are 100 – 120nm thick and are deposited at a rate of $\sim 50\text{nm}/\text{min}$ (with a pressure of 2mTorr and a power of 160W [4]). In this work we studied seven Josephson junctions with lengths ranging from 200 nm to 2000 nm. Device dimensions are listed in the supplementary information [16]. Junction A is found to be in the short regime, Junctions B and E are intermediate, while Junctions C, D, F, and G are in the long regime. Below we present primarily the data measured on four junctions A-D ($L = 200\text{nm}$, 400nm , $1\mu\text{m}$, and $2\mu\text{m}$) fabricated on the same substrate.

The junctions are measured in a four-terminal setup with the carrier density in graphene being controlled by a gate voltage, V_G . Figure 1 presents a map of the differential resistance $dV/dI(V_G, I)$, measured on Junction A at $T = 1.5$ K. The dark region of vanishing resistance indicates a supercurrent, which persists at all values of V_G . As the current is swept from the negative to the positive values, the transition from the normal to the superconducting state is seen at negative bias when $|I| = I_R$ (the retrapping current.) The transition from the superconducting back to the normal state happens

at positive bias when $I = I_S$. As commonly observed in graphene Josephson junctions, at low temperatures the samples exhibit hysteresis, $I_S \gtrsim I_R$ [22–27], which could be attributed to either underdamped junction dynamics [8, 25], or to the self-heating by the retrapping current [27, 28]. As discussed in the supplementary material, the second scenario is more likely for most of the range studied here. Based on the measurements of the switching statistics [16, 29–31], in the following we will use the switching current to represent the true critical current of the junction, I_C .

In the hole-doped regime, the reflections of ballistic charge carriers from the n-doped contact interfaces yield the quantum (“Fabry-Perot”) interference. A very similar oscillation pattern could be observed in the dependence of both the normal conductance, G_N , and the critical current I_C on gate voltage V_G (Figure 1c) [1, 2, 4]. Oscillations in normal resistance R_N are also observed as a function of bias voltage V_B (Figure 4a inset) [2, 4, 32, 33].

The critical current I_C is observed to rapidly decrease with temperature, however the functional form of $I_C(T)$ strongly depends on the length of the junction. Figure 2 shows the evolution of $I_C(T)$ from the short to the long regime. Each panel shows data measured for several values of V_G , which from here on is shown relative to the Dirac point. The shortest junction (Figure 2a) can only support a single ABS; in this regime, the current is:

$$I_C(T, \phi) \propto \frac{e\Delta}{R_N} \frac{\sin \phi}{\sqrt{1 - \tau \sin^2 \phi/2}} \tanh \left(\frac{\Delta}{2k_B T} \sqrt{1 - \tau \sin^2 \phi/2} \right) \quad (1)$$

where τ is the transmission coefficient of the S-N interface and R_N the normal state resistance. For a given

T , this expression should be maximized over ϕ to determine $I_C(T)$ [12–14]. Moreover, at higher temperatures the superconducting gap will be suppressed; we approximate the temperature dependence of the gap as $\Delta(T) \approx \Delta_0 \sqrt{1 - (T/T_C)^2}$, where Δ_0 is the gap for $T \rightarrow 0$, and T_C is the critical temperature [8, 34, 35]. Taking the complete temperature-dependent expression, we fit $I_C(T)$ for Junction A using the value $\Delta_0 = 1.2$ meV extracted from multiple Andreev reflections measurements. The fit is in excellent agreement with the data (Figure 2a).

The transmission coefficient τ extracted from the fit is plotted in the inset of Figure 3 as a function of the gate voltage. We can also estimate the transmission coefficient via an alternative method, by comparing the junction normal conductance G_N to the ballistic limit of conductance, $G_0 = Ne^2/h$, where $N = 4\sqrt{\frac{2e}{\pi}}W$ is the number of transversal modes and $n = V_G C_G/e$ is the carrier density. τ estimated as G_N/G_0 is shown in blue in the inset of Figure 3. Both methods provide consistent results, with τ in junction A reaching 90% at high densities. Furthermore, we find that the normal conductance of all junctions is very close to the ballistic limit. Figure 3a compares the normal conductance of junctions A-D normalized by junction's width (in fact, junctions A-C have the same widths). All four curves are very close to each other and approach the ballistic limit for positive gate voltages (dashed line). This result indicates two important facts: a) the contacts of all junctions are highly transparent on the n-doped side and b) the junctions' conductances do not depend on length, confirming their ballistic nature.

We now return to the critical current measured in the longer Junctions B-D. In Figure 2(b-d), I_C is plotted on a semilogarithmic scale and clearly shows exponential dependence at high temperatures T (over an order of magnitude in panels c and d). This is consistent with the expected long junction behavior $I_C \propto \exp(-k_B T/\delta E)$ [5–7, 9–11] and allows us to extract the energy scale δE . The temperature dependence eventually saturates at low temperatures, when $k_B T$ becomes comparable to δE .

Figure 3b shows that for a given device $\delta E(V_G)$ remains roughly constant as a function of V_G for both electron and hole doping, as expected in the long ballistic regime. δE is on the order of 0.05 meV for the longest device, Junction D, and goes up to ~ 0.2 meV for Junction E. While δE is consistent with the expected value of $\frac{\hbar v_F}{2\pi L}$ for Junction D, it is suppressed for shorter junctions. As the devices are ballistic, the suppression of δE cannot be explained by the effective lengthening of the carrier path due to diffusion.

To explain the suppressed δE , we observe that the previous discussion of the long junctions neglected the coherence length ξ compared to L . Taking ξ into account suppresses the level spacing, which becomes $E_0 = \frac{\pi \hbar v_F}{L + \xi}$ [36].

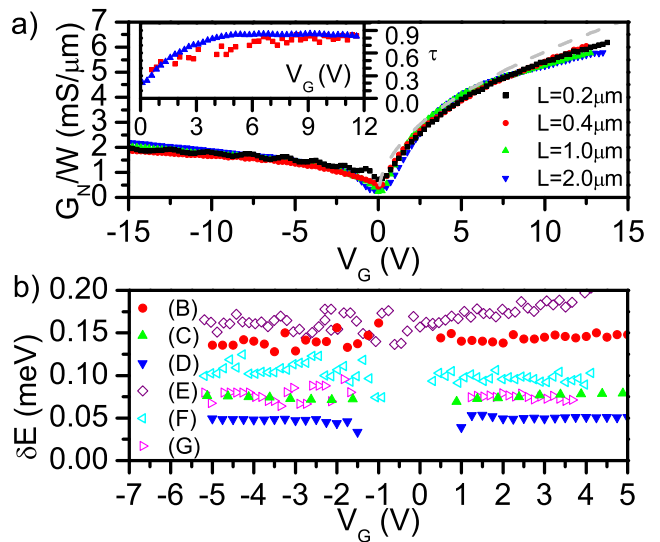


FIG. 3. a) Normal conductance of Junctions A-D normalized by the width of the junctions, G_N/W . Even though the device lengths are different by up to a factor of 10, the three curves are very close to each other, thus proving the ballistic nature of these junctions. At positive V_G , G_N of all junctions is found to approach $G_0 = Ne^2/h$ (gray dashed line), indicating consistently high contact transparency for n-doping in these devices. Inset: Transmission coefficient τ of Junction A. τ is calculated via two methods: comparing the normal conductance G_N to the ballistic limit $G_0 = Ne^2/h$ (blue), and fitting the critical current I_C vs. temperature T (red). Both methods provide consistent results and indicate high contact transparency for N-doping. b) Energy δE extracted from the slope of $\log(I_C)$ vs. T for Junctions (B-G). As expected in the long junction regime, δE depends only on device length L and is almost density-independent through both the electron and hole doping.

While the general expression for $I_C(T)$ in the $L \approx \xi$ regime is not known, numerical simulations show that it still roughly follows the $\propto \exp(-k_B T/\delta E)$ dependence, with δE suppressed by a factor of ~ 2 compared to the estimate that neglects ξ (Figure 3b in Ref. [34]). In our case, $\xi \approx 550$ nm, which explains the suppressed δE in the intermediate regime (Junctions B, E). Eventually, the junction transitions to the short regime, where the exponential dependence no longer holds.

We now turn to the saturation of I_C in the low temperature limit: $k_B T \ll \Delta_0$ for a short junction, or $k_B T \ll \delta E$ for a long junction. In the long ballistic junction regime, the $T = 0$ critical current is expected to be on the order of $e\delta E/h$ per transversal mode [7, 9, 37]. Figure 4b shows the ratio $\frac{\hbar I_C}{N e \delta E}$ as a function of the gate voltage. Strikingly, the curves for the four junctions are very close to each other and converge to a constant level of ≈ 1 at high gate voltage, where the graphene-MoRe interfaces are highly transparent. (See Supplementary for data on additional devices.) Similarly, the $T = 0$ critical current per mode is expected to be $\sim e\Delta_0/h$ in an ideal

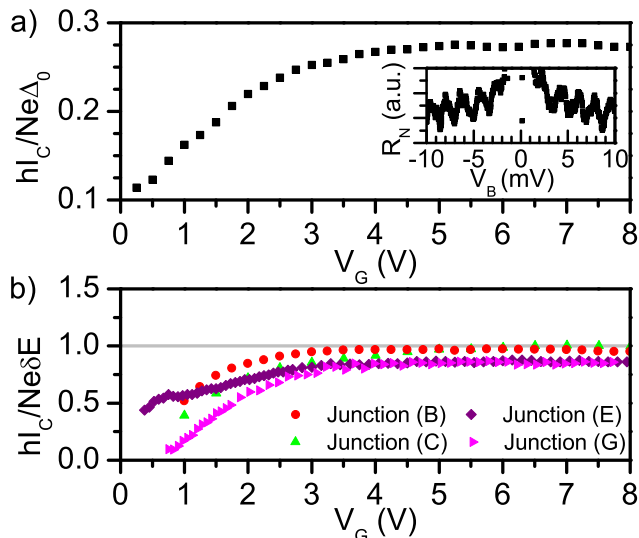


FIG. 4. a) The ratio $hI_C/Ne\Delta_0$ measured on Junction A at $T = 300\text{mK}$ as a function of V_G . The number of modes N is $W(4\sqrt{n/\pi})$, where n is the carrier density as determined from V_G . As the gate voltage increases and the transmission of the graphene-MoRe interfaces approaches 1, the plotted ratio saturates. Inset: Differential conductance versus bias voltage V_B for the 650 nm long Junction F, gated to the p-doped regime ($V_G = -4.2\text{V}$). The period of the Fabry-Perot oscillations yields the level spacing, $E_0 \approx 2\text{ meV}$, which is consistent with the expected $E_0 = 2\pi^2\delta E$ ($\delta E \approx 0.1\text{ meV}$ for this junction.) b) The ratio $hI_C/Ne\delta E$ for junctions in the long regime (B,C,E,G), measured as a function of V_G at 60mK. (See supplementary for Junction F. Junction D does not yet saturate at the base temperature.) At higher V_G the ratio converges toward a constant value in all junctions.

short junction [8, 9]. Figure 4a plots the ratio $\frac{hI_C}{Ne\Delta_0}$ for Junction A, which indeed saturates at high gate voltage, although its value ≈ 0.3 is significantly smaller than ~ 2 predicted by theory of Ref. [38]. Previous works have observed similar deviations from theory [2]. The mechanism for such suppression is unclear and can not be explained by environmental damping effects, nor the effect of imperfect transmission [16]. (Note: as there are currently no graphene-specific theoretical works predicting the ratio $\frac{hI_C}{Ne\delta E}$ in the long regime, it is unclear whether the value of ~ 1 observed in Figure 4b is coincidental.)

The ratio $\frac{hI_C}{Ne\delta E}$ is significantly reduced close to charge neutrality. This suppression most likely arises from the V_G dependence of the transmission coefficient τ of the superconductor-graphene interface. We extract the contact transparency from the junction normal resistance as h/Ne^2R_N and find that while τ is close to 1 at high densities, it does get significantly suppressed close to the charge neutrality point. Considering this suppression allows us to partially account for the reduced $\frac{hI_C}{Ne\delta E}$ ratio (see Supplementary).

In conclusion, we studied the nature of the critical current in several ballistic superconductor-graphene-

superconductor junctions. We find that in the short junction regime, $L \ll \xi$, the critical current follows eq. (1), while in the intermediate and long junctions I_C is $\propto e^{-k_B T/\delta E}$. The slope of $\log I_C$ vs. T dependence allows us to extract the energy scale δE , which depends on the junction length but not the gate voltage V_G . While consistent for very long junctions $L \gg \xi$, the values of δE for intermediate devices $L \sim \xi$ are smaller than those naively estimated from the junction lengths. We attribute this suppression to the finite coherence length. Finally, we show that at the lowest temperature, I_C saturates at a level determined by the product of Δ_0 or δE (depending on the regime), and the number of transversal modes across the junction width. Our observations demonstrate the universality of the critical current in several regimes relevant to most hybrid superconductor-encapsulated graphene devices.

I.V.B. and M.Y. acknowledge the Canon foundation. C.T.K., M.T.W., A.S., and G.F. were supported by ARO Award W911NF-16-1-0122. F.A. acknowledges the ARO under Award W911NF-14-1-0349. A.W.D. was supported by the NSF graduate research fellowship DGF1106401. Low-temperature measurements performed by G.F. were supported by the Division of Materials Sciences and Engineering, Office of Basic Energy Sciences, U.S. Department of Energy, under Award DE-SC 0002765. This work was performed in part at the Duke University Shared Materials Instrumentation Facility (SMIF), a member of the North Carolina Research Triangle Nanotechnology Network (RTNN), which is supported by the National Science Foundation (Grant ECCS-1542015) as part of the National Nanotechnology Coordinated Infrastructure (NNCI). M.Y. acknowledges financial support by Grant-in-Aid for Scientific Research on Innovative Areas “Science of Atomic Layer”. M.Y. and S.T. acknowledge support by Grant-in-Aid for Scientific Research S (No. 26220710), and Grant-in-Aid for Scientific Research A (No. 26247050).

We would like to thank Konstantin Matveev for fruitful discussions.

-
- [1] V. E. Calado, S. Goswami, G. Nanda, M. Diez, A. R. Akhmerov, K. Watanabe, T. Taniguchi, T. M. Klapwijk, and L. M. K. Vandersypen, *Nature Nano.* **10**, 761-764 (2015).
 - [2] M. Ben Shalom, M. J. Zhu, V. I. Fal’ko, A. Mishchenko, A. V. Kretinin, K. S. Novoselov, C. R. Woods, K. Watanabe, T. Taniguchi, A. K. Geim, and J. R. Prance, *Nature Phys.* **12**, 318-322 (2016).
 - [3] M. T. Allen, O. Shtanko, I. C. Fulga, J. I. J. Wang, D. Nurgaliev, K. Watanabe, T. Taniguchi, A. R. Akhmerov, P. Jarillo-Herrero, L. S. Levitov, and A. Yacoby, *Nature Phys.* **12**, 128-133 (2016).
 - [4] F. Amet, C. T. Ke, I. V. Borzenets, Y. Wang, K. Watanabe, T. Taniguchi, R. S. Deacon, M. Yamamoto, Y.

- Bomze, S. Tarucha, and Finkelstein, *Science* **352** (6288), p.966 (2016).
- [5] I.O. Kulik, *Sov. Phys. JETP* **30**, 944 (1970).
- [6] J. Bardeen and J. L. Johnson, *Phys. Rev. B* **5**, 72 (1972).
- [7] A. V. Svidzinskii, *Spacially-Inhomogeneous Problems of Theory of Superconductivity* (Nauka, Moscow, 1982).
- [8] M. Tinkham, *Introduction To Superconductivity* (McGraw-Hill, New York, 1996).
- [9] A. A. Golubov, M. Yu. Kupriyanov, and E. Iliichev, *Rev. Mod. Phys.* **76**, 411 (2004).
- [10] A. V. Svidzinsky, T. N. Antsygina, and E. N. Bratus, *Sov. Phys. JETP* **3**, 860 (1972).
- [11] A. V. Svidzinsky, T. N. Antsygina, and E. N. Bratus, *J. Low Temp. Phys.* **10**, 131-136 (1973).
- [12] C. W. J. Beenakker, *Transport Phenomena in Mesoscopic Systems* pp.235-253 (Springer, Berlin, 1992).
- [13] C. W. J. Beenakker and H. van Houten, *Phys. Rev. Lett.* **66**, 3056 (1991).
- [14] G.-H. Lee, S. Kim, S.-H. Jhi, and H.-J. Lee, *Nature Commun.* **6**, 6181 (2015).
- [15] L. Wang, I. Meric, P. Y. Huang, Q. Gao, Y. Gao, H. Tran, T. Taniguchi, K. Watanabe, L. M. Campos, D. A. Muller, J. Guo, P. Kim, J. Hone, K. L. Shepard, and C. R. Dean, *Science* **342**, 614-617 (2014).
- [16] See Supplementary Information, which includes Refs.17–21.
- [17] T. A. Fulton and L. N. Dunkleberger, *Phys. Rev. B* **9**, 4760 (1974).
- [18] J. Clarke, E. A. Cleland, H. M. Devoret, D. Esteve, and M. J. Martinism, *Science* **239**, (1988).
- [19] M. Yu. Kupriyanov and V. F. Lukichev, *Zh. Eksp. Teor. Fiz.* **94**, 139-149 (1988).
- [20] Y. Luh, *Acta Phys. Sin.* **21**, 75 (1965); H. Shiba, *Prog. Theor. Phys.* **40**, 435 (1968); A. I. Rusinov, *Sov. Phys. JETP* **29**, 1101 (1969).
- [21] G. Eilenberger, *Z. Phys.* **214**, 195-213 (1968).
- [22] H. B. Heersche, P. Jarillo-Herrero, J. B. Oostinga, L. M. K. Vandersypen, and A. F. Morpurgo, *Nature* **446**, 56 (2007).
- [23] X. Du, I. Skachko, and E. Y. Andrei, *Phys. Rev. B* **77**, 184507 (2007).
- [24] C. Ojeda-Aristizabal, M. Ferrier, S. Guéron, and H. Bouchiat, *Phys. Rev. B* **79**, 165436 (2009).
- [25] I. V. Borzenets, U. C. Coskun, S. J. Jones, and G. Finkelstein, *Phys. Rev. Lett.* **107**, 137005 (2011).
- [26] I. V. Borzenets, U. C. Coskun, S. J. Jones, and G. Finkelstein, *IEEE Trans. Appl. Supercond.* **22**, 1800104 (2012).
- [27] I.V. Borzenets, U.C. Coskun, H.T. Mebrahtu, Yu.V. Bomze, A.I. Smirnov, and G. Finkelstein, *Phys. Rev. Lett.* **111**, 027001 (2013).
- [28] H. Courtois, M. Meschke, J. T. Peltonen, and J. P. Pekola, *Phys. Rev. Lett.* **101**, 067002 (2008).
- [29] U.C. Coskun, M. Brenner, T. Hymel, V. Vakaryuk, A. Levchenko, and A. Bezryadin, *Phys. Rev. Lett.* **108**, 097003 (2012).
- [30] G.-H. Lee, D. Jeong, J.H. Choi, Y.-J. Doh, and H.-J. Lee, *Phys. Rev. Lett.* **107**, 146605 (2011).
- [31] C. T. Ke, I. V. Borzenets, A. W. Draelos, F. Amet, Yu. Bomze, G. Jones, M. Craciun, S. Russo, M. Yamamoto, S. Tarucha and G. Finkelstein, *Nano Lett.* **16** (8), 4788 (2016).
- [32] A. F. Young, and P. Kim, *Nature Phys.* **5**, 222-226 (2009).
- [33] P. Rickhaus, R. Maurand, M.-H. Liu, M. Weiss, K. Richter, and C. Schenberger, *Nature Commun.* **4**, 2342 (2013).
- [34] I. Hagymasi, A. Kormanyos, and J. Cserti, *Phys. Rev. B* **82**, 134516 (2010).
- [35] R. Dougherty, J. D. Kimel, *Superconductivity Revisited*, (CRC Press, London 2013).
- [36] P. F. Bagwell, *Phys. Rev. B* **46**, 12573-12586 (1992).
- [37] C. Ishii, *Prog. Theor. Phys.* **44**, 1525 (1970).
- [38] M. Titov and C. W. J. Beenakker, *Phys. Rev. B* **74**, 041401(R) (2006).